NANO LETTERS

2002
Vol. 2, No. 9
983−987

Size-Dependent Photoconductivity in CdSe Nanoparticles as Measured by Time-Resolved Terahertz Spectroscopy

Matthew C. Beard, Gordon M. Turner, and Charles A. Schmuttenmaer*

Department of Chemistry, Yale University, 225 Prospect Street, P.O. Box 208107, New Haven, Connecticut 06520-8107

Received May 22, 2002; Revised Manuscript Received July 25, 2002

ABSTRACT

The size-dependent transient photoconductivity in CdSe nanoparticles (NPs) has been investigated using time-resolved THz spectroscopy (TRTS). We find that the mobility increases with an r^4 dependence for NPs in the strong confinement regime and is governed by a restricted mean free path for NPs in the weak confinement regime. The photoexcited carriers undergo ballistic transport to the surface of the NPs. The average number of electron–hole pairs generated in the NPs falls into three distinct groupings based on the NP radius.

The photoconductivity and charge transport properties of semiconductor nanoparticles (NPs) are critically important with regard to their use in electrooptic devices.[1] Measuring the photoconductivity in NPs, however, is a challenging problem because of the inherent difficulty of attaching wires to nanometer-sized objects. Furthermore, picosecond (ps) carrier dynamics play an important role in efficient charge separation and transport, but the low temporal resolution of traditional methods used to determine the photoconductivity precludes their use in studying sub-ps to ps dynamics. Time-resolved THz spectroscopy (TRTS), on the other hand, is a noncontact electrical probe capable of measuring the photoconductivity on a sub-ps to nanosecond (ns) time scale.[2,3] In this letter, TRTS is employed to study the photoconductivity in CdSe NPs of various sizes.

Semiconductor NPs have sustained tremendous interest in the chemistry and physics communities because of dramatic size-dependent effects. As the physical dimensions of NPs approach molecular dimensions, quantization effects become important and many bulk properties become size dependent. The most well documented example is that the band gap increases as the particle size decreases, shifting the absorption and luminescence spectra to the blue.[4,5] Size-dependent redox potentials,[6] lattice constants, fluorescence Stokes shifts,[7] and phase transitions, such as the pressure induced structural transition[8] and melting point,[9] have also been observed.

The scaling laws that govern the size-dependent phenomena do not all have the same form. For example, it has been found that the band gap decreases as $1/r^2$ while the melting temperature increases as $1/r$, where r is the radius of the nanoparticle.[4,5,9] The scaling laws relate to changes in the properties of the material and, in general, result from either a quantum confinement effect, as in the case of the band gap, or an increasing surface-to-volume ratio, as in the case of the melting temperature. The surface of the nanoparticle plays an increasingly important role as their size decreases.

The experiments described here consist of generating charge carriers in the NPs with above band gap photoexcitation (3.1 eV), and then probing them with low-energy far-infrared (FIR) light (0.1 to 3 THz or equivalently 0.4 to 12 meV). The FIR transmission is directly related to the photoconductivity of the material.[2,3] The probe photon energies used in a TRTS experiment are much smaller than those employed in visible or IR time-resolved experiments and are only sensitive to intra-sub band transitions. Measurements of the dc conductivity have been made in nanoparticles by attaching wires to them, and the well-known Coulomb blockade and Coulomb staircase resulting from the charging energy needed to add additional carriers to the nanoparticle have been observed.[7,10,11] However, such measurements do not provide information about the conductivity within the nanoparticle. Furthermore, photoexcitation creates electron−hole (e−h) pairs rather than single electrons and can excite multiple e−h pairs within the same NP[12] without concern for the charging effects present in the dc conductivity measurements.

The goal of this work is to investigate the size-dependent photoconductivity in semiconductor NPs. The conductivity is affected primarily by two fundamental length scales: the Bohr exciton radius a_B, and the carrier mean free path l_f. The Bohr exciton radius defines the spatial extent of the e−h pair and is defined as $a_B = \hbar^2\epsilon/(m^*e^2)$ where m^* is the effective mass of the exciton, and ϵ is the dielectric

* Corresponding author. E-mail: charles.schmuttenmaer@yale.edu

10.1021/nl0256210 CCC: $22.00
Published on Web 08/14/2002

constant.[13] For CdSe $a_B = 4.9$ nm based on an electron effective mass of 0.13 m_e and a hole effective mass of 0.45 m_e.[14] Quantum size effects are most pronounced when the size of the NPs becomes smaller than a_B because of the physical confinement of the e−h pair. At these sizes, carrier transport within the NPs in the traditional sense is no longer a meaningful concept as the electron is delocalized over the entire NP. However, we expect a smooth transition from bulk behavior to that of the confined system.

The length scale that governs bulk carrier transport is the carrier mean free path, l_f. The mean free path is the length that the carriers travel on average before suffering a collision, and $l_f = \nu\tau$ where ν is the thermal carrier velocity and τ is the average time between collisions. The collisions cause a momentum randomization analogous to atoms diffusing in a gas. In bulk CdSe the mean free path of an electron is ∼20 nm and it is ∼11 nm for a hole. At NP diameters smaller than or comparable to l_f there is an effective mean free path given by[15]

$$\frac{1}{l_{eff}} = \frac{1}{r} + \frac{1}{l_f} \tag{1}$$

If we assume the velocity of the carriers remains the same as that in the bulk, then the scattering time is decreased, $\tau' = l_{eff}/\nu$, and this manifests itself as a reduction in the mobility, $\mu' = e\tau'/m^*$. Therefore, as the NP diameter decreases, the mobility should decrease with a dependence given by $\mu' \propto rl_f/(r + l_f)$.

As discussed elsewhere, the TRTS experimental setup consists of a visible pump pulse followed by a THz probe pulse.[2,3] Photogeneration of carriers is achieved with 400 nm light, which is above the band gap in all of the NP sizes used in this study. The pump pulse energy was typically 100 μJ/pulse, and the spot size was ∼1 cm diameter.

Nearly monodisperse samples with sizes ranging from 2.54 to 25 nm were prepared by the method developed by Peng et al.[16,17] The sizes of the nanoparticles were determined from the exciton peak in the UV−vis spectra.[18] Transmission electron microscopy (TEM) was used to assess the NP monodispersity and quality. Monodispersities were estimated to be ∼10%. The NPs were dispersed in toluene for the work reported here. However, NPs suspended in chloroform and poly(vinyl butyral) were also studied, and the results depend only on the size of the nanoparticle and not on the matrix or solvent chosen. The measured signal was independent of the NP concentration as long as the pump pulse was completely absorbed. Thus, NP suspensions in a 1 mm path length cuvette were prepared with an optical density (OD) at the pump wavelength of about 5. We do not observe appreciable changes in the NP UV−vis absorption spectra or TEM images after long exposure to the pump beam.

In this paper we present size-dependent carrier dynamics as determined from TRTS pump scans and size-dependent conductivity as determined from TRTS probe scans.[2,3] A TRTS pump scan is collected by monitoring the most positive feature of the ΔTHz waveform as the pump delay is varied, and this is interpreted as the average THz transient response.

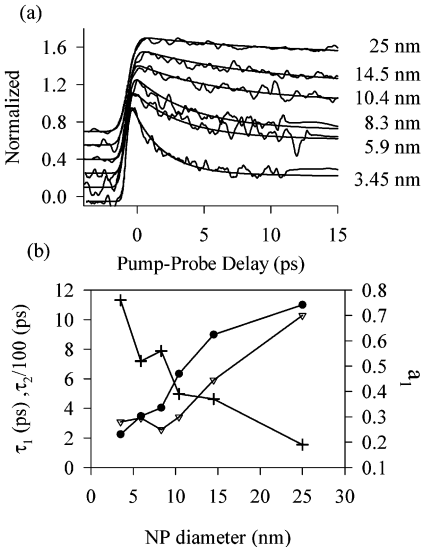

Figure 1. (a) TRTS pump scans for the eight sizes of CdSe NPs, normalized and offset from smallest to largest size NP. All transients are well fit by a biexponential function convoluted with a Gaussian function (smooth lines). (b) Best fit parameters: ● = τ_1; ▽ = τ_2/100; + = a_1. A linear dependence with diameter is observed for all three parameters.

We measure an instrument response limited onset, followed by a biexponential decay. This finding is similar to other time-resolved measurements in semiconductor NPs where one to three exponential decays are observed.[12,19−27] TRTS probe scans are obtained by collecting the entire transmitted THz pulse at a given pump−probe delay time. A Fourier transform is then performed, and the frequency-dependent change in optical density (ΔOD) and change in phase ($\Delta\phi$) are obtained. The frequency-dependent information provides a great deal of information regarding the conduction mechanism.[2,3,28,29]

There has been much effort extended to understand carrier dynamics in semiconductor NPs, and many ultrafast time-resolved techniques have been employed in this quest.[19,21−24,30] The visible pump−IR pump−IR probe experiments of Guyot-Sionnest and co-workers[19] are the most similar to our TRTS experiments. A visible pulse creates e−h pairs, which are allowed to equilibrate in the conduction band. A time-resolved IR pump−IR probe experiment is then performed at least 10 ps after the visible pulse. The IR pulses are tuned to the intraband $1S_e-1P_e$ transition, and, therefore, are only sensitive to conduction band electrons. TRTS experiments, on the other hand, probe valence (hole) dynamics because the probe photon energies are too small for absorption by the $1S_e-1P_e$ transition. Comparing and contrasting TRTS results with those of other ultrafast experiments provides new insights not obtainable from either type of experiment. In particular, it has become apparent in recent years that investigating both the electron and the hole dynamics are essential in understanding the energy relaxation pathways in these materials.[22,31]

Figure 1a shows normalized TRTS pump scans for a variety of NP sizes at a constant pump fluence. The data are

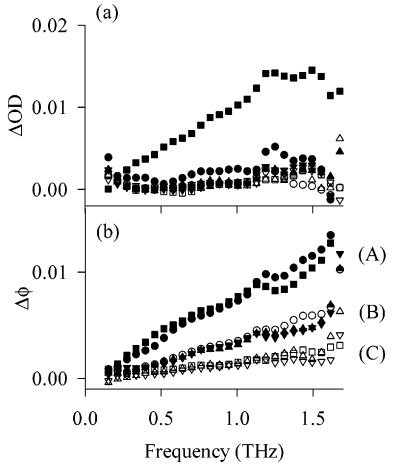

Figure 2. (a) ΔOD and (b) $\Delta\phi$ for CdSe NPs. ▽ = 2.54 nm, △ = 3.45 nm, □ = 3.57 nm, ○ = 5.9 nm, ▼ = 8.3 nm, ▲ = 10.4 nm, ■ = 15.4 nm, and ● = 25 nm. The $\Delta\phi$ group is divided into three groups. (A) 25 nm, and 15.4 nm; (B) 10.4, 8.3, and 5.9 nm; and (C) 3.57, 3.45, and 2.5 nm.

fit well by a biexponential decay convoluted with a Gaussian function that represents the onset of photoconductivity,

$$y = \{a_1 \exp[-(t - t_0)/\tau_1] + a_2 \exp[-(t - t_0)/\tau_2]\} \otimes G(t - t_0) \quad (2)$$

where $a_1 + a_2 = 1$, τ_1 and τ_2 are the exponential time constants, $\otimes$ represents a convolution, and $G(t - t_0)$ is a Gaussian function centered at t_0 with fwhm of ~600 fs and represents the instrument response time for TRTS pump experiments.[2,3] Figure 1b displays the extracted parameters plotted as a function of NP diameter. Both the fast and slow time constants increase linearly with the NP diameter. The amplitude of the fastest time constant decreases with increasing diameter.

We attribute the linear lifetime dependence to a ballistic transport mechanism. Carriers are predominantly trapped at the surface of the NPs. Carriers undergoing diffusive transport to the surface would exhibit a quadratic dependence on their lifetime with NP radius. The mean free path in bulk CdSe is 20 nm, which is larger than the NP diameters studied. Therefore, carriers scatter off the surface of the NPs many times before being trapped.

The dependence of the TRTS response on the pump power was performed (not shown) and the results are qualitatively consistent with previous observations.[19,32] At the earliest times, several ps after photoexcitation, the THz transient is linear in pump power, while at the longest times, tens to hundreds of ps, there is a saturation of the signal with pump power.

The TRTS response does not depend on the relative polarization between pump and probe beams, both of which are linearly polarized. The lack of a polarization dependence results from the small probe photon energies (1−10 meV) such that only valence (hole) states are probed. The hole wave function is spread out over many densely spaced valance band states.[31] In contrast, a polarization dependence is observed in the visible pump−IR pump−IR probe experiments[19] where the conduction band $1S_e-1P_e$ transition is probed.

Figure 2 shows the change in optical density, ΔOD, and change in phase, $\Delta\phi$, as a function of frequency 1 ps after photoexcitation. Surprisingly, a distinct grouping appears in the plot of $\Delta\phi$ and is also present when viewing the integrated intensity of the time-domain THz difference pulse (not shown). The NPs separate into three groups: (A) diameters greater than 15 nm; (B) diameters that span 5.9−10.4 nm; and (C) diameters that span 2.5−3.6 nm. The ΔOD, on the other hand, is small and essentially constant for all of the NP sizes except for an anomalous, yet reproducible, behavior observed for the 15.4 nm diameter sample.

The NPs are dispersed in toluene and we employ a model to extract the photoconductivity. We treat the sample as dielectric inclusions embedded in toluene and use Bruggeman effective medium theory,[33]

$$\eta_{tol}\left(\frac{\epsilon_{tol} - \epsilon}{\epsilon_{tol} + 2\epsilon}\right) + \eta_{CdSe}\left(\frac{\epsilon_{CdSe} - \epsilon}{\epsilon_{CdSe} + 2\epsilon}\right) = 0 \quad (3)$$

where $\eta_{tol,CdSe}$ is the volume fraction of toluene or the NPs and $\eta_{tol} + \eta_{CdSe} = 1$, ϵ_{tol} is the permittivity of toluene and is known from static THz measurements,[34] ϵ is the effective, or measured permittivity of the composite medium, and ϵ_{CdSe} is the permittivity for either the photoexcited NPs or static CdSe. We assume that the CdSe static permittivity is identical to that measured for bulk CdSe.[35] Photoexcitation is assumed to create charge carriers; the photoexcited permittivity is calculated using $\epsilon = \epsilon_{static} + i\sigma/\epsilon_o\omega$, where σ is the complex conductivity and ϵ_0 is the permittivity of free space.

We employ the Drude model to represent the conductivity of the carriers in the NPs. It is the simplest model of conductivity and is described by

$$\sigma(\omega) = \frac{\epsilon_0 \omega_p^2 \tau}{(1 - i\omega\tau)} \quad (4)$$

where ω is the radial frequency, τ is the average time between collisions, and the plasma frequency ω_p is obtained from $\omega_p^2 = Ne^2/(\epsilon_0 m^*)$, where N is the carrier density, e is the charge of an electron, and m^* is the carrier effective mass.

The model contains two free parameters, τ, and J, where J is the fluence of the excitation pulse in photons/cm^2. The carrier density and volume fraction of the photoexcited NPs are determined from J. The nonuniform distribution of photoexcited NPs created by the excitation pulse is accounted for explicitly in the simulation. The fluence J decreases exponentially as the pulse travels into the sample. In the simulation, the sample space is divided into n slabs of thickness dx such that $n \times dx = 1$ mm (thickness of the cuvette), and n is typically ~100. Within each slab the average e−h occupation number of excited NPs $\langle N'_{e-h}\rangle$ is calculated from a modified Poisson distribution.[36] The total number of excited NPs in the slab dx is determined from the number of photons absorbed in the slab divided by

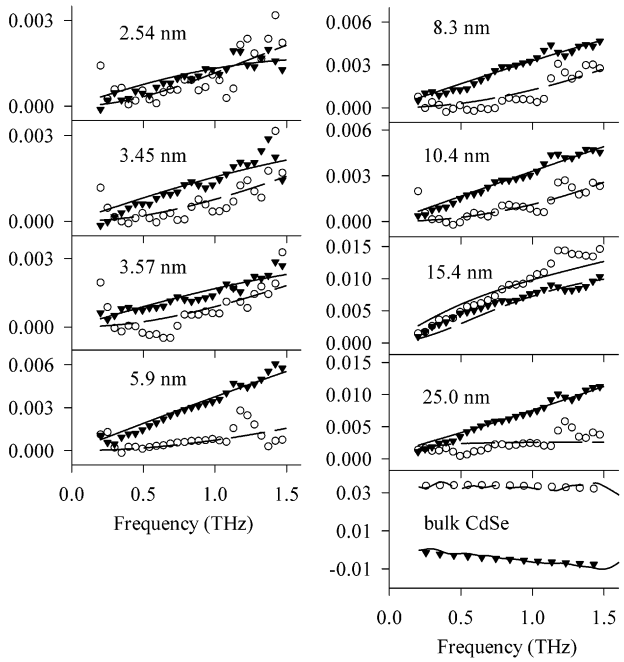

Figure 3. Values of the frequency-dependent ΔOD and $\Delta\phi$ for the eight CdSe NPs and bulk CdSe. The smooth lines are the results of a nonlinear least-squares fit of the model described in the text to the measured data of Figure 2. The open symbols and dashed lines are ΔOD and the filled symbols and solid lines are $\Delta\phi$. The ΔOD and $\Delta\phi$ when photoexciting bulk CdSe are also shown for comparison.

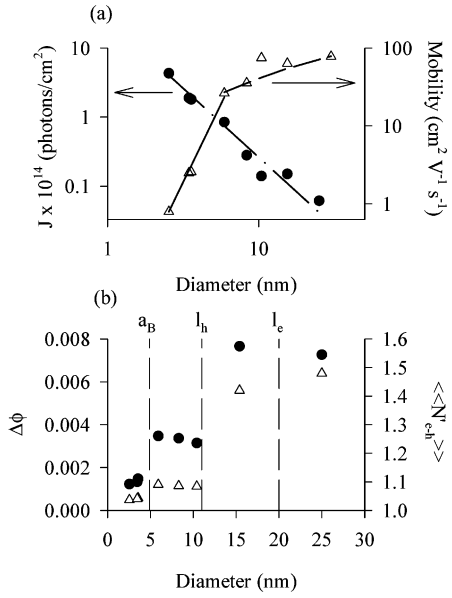

Figure 4. (a) A log−log plot of the extracted parameters J and mobility. The effective photon fluence has a $1/r^2$ dependence (dash−dotted line and ●). The mobility (△) varies as r^4 (solid line) for diameters < 5.9 nm and $\mu \propto rl_f/(r + l_f)$ (dashed line) for diameters > 5.9 nm with $l_f = 13.0$ nm. (b) The value of $\Delta\phi$ at 1 THz from Figure 3 plotted vs NP diameter (●). The average occupation number $\langle\langle N'_{e-h}\rangle\rangle$ extracted from the model (△). Vertical lines are drawn in at the exciton radius $a_B = 4.9$ nm, the bulk hole mean free path $l_h = 11$ nm, and the bulk electron mean free path $l_e = 20$ nm.

$\langle N'_{e-h}\rangle$. The total number of excited NPs in the slab is multiplied by the volume of an individual NP and is divided by the total volume of the slab (visible spot size × dx) to obtain the volume fraction in each slab. The carrier density, N, is found within each slab by dividing $\langle N'_{e-h}\rangle$ by the NP volume. This explicitly accounts for the Poisson distribution of e−h pairs excited within each slab. The change in optical density and change in phase for the THz probe pulse are determined from the complex transmission coefficient calculated for a dielectric stack of the n slabs.[37] The samples are assumed to have an OD of 5 at 400 nm, but the results of the simulation are independent of the exact OD, as long as it is greater than 2 (all the excitation photons are absorbed).

Figure 3 shows the results of a nonlinear least-squares fit of the model to the data for the eight samples studied. Even the "anomalous" 15.4 nm sample is fit by the model, but not as well as for the other samples. The fits are very robust with uncertainties of <5% in the extracted parameters. We have also employed a model that incorporates a resonance absorption based on the Kohn model,[38] and we investigated models that allow for backscattering and/or charge localization,[39] but find that incorporating the Drude model performs best. The transient photoconductivity of a 1 mm thick single crystal (0001) CdSe (RMT Ltd.) was measured for comparison, and the ΔOD and $\Delta\phi$ are shown along with a Drude model fit. The extracted mobility in the bulk is 470 cm^2 V^{-1} s^{-1} at a carrier density of 2.2×10^{18} cm^{-3}.

Figure 4a plots the extracted mobility on a log−log scale for each of the NP samples; the mobility is related to the scattering time through $\mu = e\tau/m_h^*$. The mobility depends markedly on the size of the NPs. For diameters <5.9 nm the mobility varies as r^4 (solid line), for diameters >5.9 nm the mobility approaches a limiting value with a $\mu \propto rl_f/(r + l_f)$ dependence (dashed line). A best fit produces a value of 13.0 nm for the mean free path, l_f. The bulk hole mobility is predicted to be $\mu_h(r \rightarrow \infty) = 145$ cm^2 V^{-1} s^{-1}. Assuming the electrons and holes have the same collision time, τ, the bulk electron mobility is $\mu_e(r \rightarrow \infty) = \mu_h(r \rightarrow \infty) \times m_h^*/m_e^* = 502$ cm^2 V^{-1} s^{-1}, in good agreement with the measured bulk mobility in CdSe.

During the fit, the photon fluence J was allowed to float to obtain the best results. Figure 4a also displays the extracted values of the effective J as a function of NP diameter, and it decreases with a $1/r^2$ dependence (dash-dotted line). The size-dependence of J indicates there is a contribution to the signal not accounted for in the model (the measurements were performed at a constant J). There are several possible reasons why J shows a size dependence. In large NPs there may exist e−h pairs that do not contribute to the signal, because they are not conductive. Alternatively, in small NPs the e−h pairs may be more polarizable than in large ones and thereby contribute more to the signal.

Figure 4b shows the value of $\Delta\phi$ at 1 THz as a function of NP diameter. The values fall into three groups: NPs in the weak ($d > a_B$) or strong ($d < a_B$) confinement regimes, where $a_B = 4.9$ nm, and a third group occurs for sizes larger than the bulk hole mean free path, $l_h = 11$ nm. To verify this interpretation of the groupings, we propose measuring

the photoconductivity in CdS NPs, where the Bohr radius is $a_B = 2.8$ nm and the groupings should occur at different NP diameters.

For the smallest sizes, $d < a_B$ the electron is completely delocalized and not conductive. However, the hole has a Bohr radius of $a_h = 1.1$ nm and remains conductive at all NP sizes studied. In the intermediate size regime $a_B < d < l_h$, excitonic states exist, but the THz radiation probes only the hole states. In the largest sizes, $d > l_h$, the exciton is ionized and the electron can absorb THz radiation as the bulk band structure begins to form.

It is informative to view the average e−h pairs created for each sample (this is obtained by averaging the $\langle N'_{e-h}\rangle$ for the n stacks in the simulation). Figure 4b also displays this value for each sample. Even for the largest sizes the average number of e−h pairs per NP is < 2. The average volume fraction also falls into distinct groups (not shown). These groupings occur because of the interplay between the decreasing effective fluence, the increasing absorption cross section, and because photoexcitation cannot generate a fractional e−h pair.

We have measured the size-dependent photoconductivity in CdSe NPs using time-resolved THz spectroscopy. TRTS provides dynamical information similar to other ultrafast optical spectroscopic techniques, yet differs in two fundamental ways. (1) TRTS measures the dynamics in the valence band for the smallest sizes, since the probe photon energies are too small to induce transitions in the conduction band. (2) TRTS measures the transport properties within the NPs, not between the NPs, and does so in a noncontact fashion. This provides an unprecedented level of detail regarding the microscopic carrier dynamics in these materials.

We observe that the photoexcited e−h pairs decay with a biexponential time-dependence and that both time constants increase linearly with increasing NP radius. This suggests ballistic transport to the surface of the NPs. Furthermore, carriers must scatter many times before being trapped by the surface, since they reach the surface in tens of femtoseconds rather than on a picosecond time scale. Finally, the frequency-dependent measurements display a distinct grouping as a function of NP size. The mobility is found to obey an r^4 dependence for NPs whose diameters are less than a_B, and for NPs whose diameters are greater than a_B the mobility is governed by a restricted mean free path for the carriers.

Acknowledgment. The authors acknowledge the National Science Foundation and the Sloan Foundation for partial support of this research.

References

(1) Nozik, A. *J. Annu. Rev. Phys. Chem.* **2001**, *52*, 193−231.
(2) Beard, M. C.; Turner, G. M.; Schmuttenmaer, C. A. *J. Appl. Phys.* **2001**, *90*, 5915−5923.
(3) Beard, M. C.; Turner, G. M.; Schmuttenmaer, C. A. *Phys. Rev. B* **2000**, *62*, 15764−15777.
(4) Efros, A. L. *Sov. Phys. Semicond.-USSR* **1982**, *16*, 772−775.
(5) Brus, L. E. *J. Chem. Phys.* **1984**, *80*, 4403−4409.
(6) Brus, L. E. *J. Chem. Phys.* **1983**, *79*, 5566−5571.
(7) Norris, D. J. *Measurement and Assignment of the Size-Dependent Optical Spectrum in Cadmium Selenide (CdSe) Quantum Dots*, Ph.D. Thesis, Massachusetts Institute of Technology, 1995.
(8) Tolbert, S. H.; Alivisatos, A. P. *Science* **1994**, *265*, 373−376.
(9) Goldstein, A. N.; Echer, C. M.; Alivisatos, A. P. *Science* **1992**, *256*, 1425−1427.
(10) Jiang, P.; Liu, Z. F.; Cai, S. M. *Surf. Sci.* **2001**, *486*, L507-L512.
(11) Vanbentum, P. J. M.; Smokers, R. T. M.; Vankempen, H. *Phys. Rev. Lett.* **1988**, *60*, 2543−2546.
(12) Klimov, V. I. *J. Phys. Chem. B* **2000**, *104*, 6112−6123.
(13) Heath, J. R.; Shiang, J. *J. Chem. Soc. Rev.* **1998**, *27*, 65−71.
(14) Gaponenko, S. V. *Optical Properties of Semiconductor Nanocrystals*; Cambridge University Press: New York, 1998.
(15) Ashcroft, N. W.; Mermin, N. D. *Solid State Physics*; Saunders College Publishing: New York, 1976.
(16) Qu, L.; Peng, Z. A.; Peng, X. *Nano Lett.* **2001**, *1*, 333−337.
(17) Peng, Z. A.; Peng, X. G. *J. Am. Chem. Soc.* **2001**, *123*, 183−184.
(18) Dushkin, C. D.; Saita, S.; Yoshie, K.; Yamaguchi, Y. *Adv. Colloid Interface Sci.* **2000**, *88*, 37−78.
(19) Guyot-Sionnest, P.; Shim, M.; Matranga, C.; Hines, M. *Phys. Rev. B* **1999**, *60*, R2181−R2184.
(20) Klimov, V. I.; McBranch, D. W.; Leatherdale, C. A.; Bawendi, M. G. *Phys. Rev. B* **1999**, *60*, 13740−13749.
(21) Klimov, V. I.; Mikhailovsky, A. A.; McBranch, D. W.; Leatherdale, C. A.; Bawendi, M. G. *Phys. Rev. B* **2000**, *61*, R13349−R13352.
(22) Burda, C.; Link, S.; Mohamed, M.; El-Sayed, M. A. *J. Phys. Chem. B* **2001**, *105*, 12286−12292.
(23) Landes, C.; Burda, C.; Braun, M.; El-Sayed, M. A. *J. Phys. Chem. B* **2001**, *105*, 2981−2986.
(24) Underwood, D. F.; Kippeny, T.; Rosenthal, S. J. *J. Phys. Chem. B* **2001**, *105*, 436−443.
(25) Klimov, V. I.; Schwarz, C. J.; McBranch, D. W.; Leatherdale, C. A.; Bawendi, M. G. *Phys. Rev. B* **1999**, *60*, R2177−R2180.
(26) Landes, C. F.; Braun, M.; El-Sayed, M. A. *J. Phys. Chem.* **2001**, *105*, 10554−10558.
(27) Burda, C.; Link, S.; Mohamed, M. B.; El-Sayed, M. A. *J. Chem. Phys.* **2002**, *116*, 3828−3833.
(28) Turner, G. M.; Beard, M. C.; Schmuttenmaer, C. A., unpublished results, 2002.
(29) Lee, K. H.; Menon, R.; Yoon, C. O.; Heeger, A. *J. Phys. Rev. B* **1995**, *52*, 4779−4787.
(30) Klimov, V. I.; McBranch, D. W. *Phys. Rev. Lett.* **1998**, *80*, 4028−4031.
(31) Xu, S.; Mikhailovsky, A. A.; Hollingsworth, J. A.; Klimov, V. I. *Phys. Rev. B* **2002**, *65*, 045319.
(32) Klimov, V. I.; Mikhailovsky, A. A.; McBranch, D. W.; Leatherdale, C. A.; Bawendi, M. G. *Science* **2000**, *287*, 1011−1013.
(33) Choy, T. C. *Effective Medium Theory*; Clarendon Press: New York, 1999.
(34) Beard, M. C.; Schmuttenmaer, C. A. *J. Chem. Phys.* **2001**, *114*, 2903−2909.
(35) Beard, M. C. *Time-resolved THz spectrsocopy: charge transfer, solvent dynamics, and photoconductivity*, Ph.D. Thesis, Yale University, 2002.
(36) For a given J the average number of e−h pairs per NP, $\langle N_{e-h}\rangle$, is $\langle N_{e-h}\rangle = \sigma J$ where σ is the NP absorption cross section at 400 nm (see ref 12). We consider only those NPs that have been photoexcited, therefore, this number is rescaled to exclude the $m = 0$ case in the Poisson distribution. Thus $\langle N'_{e-h}\rangle = \sum_{m=1}^{\infty} mP'(m)$, where $P'(m)$ is the Poisson distribution with the $m = 0$ case removed and rescaled such that $\sum_{m=1}^{\infty} mP'(m) = 1$.
(37) To calculate ΔOD and $\Delta\phi$ the measured signal is related to the permittivity of the photoexcited and nonphotoexcited media. A THz pulse that has propagated through an absorbing material with thickness d is related to the input THz pulse E_0 by $E(\omega,d) = tE_o(\omega,0)$, where t is the complex transmission coefficient. The complex transmission coefficient for a wave incident on an n-layered dielectric stack is[40] $1/t = \Pi_{j=1}^{j=n-1}[(Z_{j+1} + Z_{in}^{(j)})/(Z_j + Z_{in}^{(j)})]\exp(-ik_jd_j)$, where the impedance of the jth stack is $Z_j = \omega/(ck_j)$, d_j is the thickness of the jth stack, k is the complex wavevector, related to the permittivity, ϵ, by $k = \omega\sqrt{\epsilon}/c$, the input impedance is[40] $Z_{in}^{(j)} = \{[Z_{in}^{(j-1)} - iZ_j\tan(k_jd_j)]/[Z_j - iZ_{in}^{(j-1)}\tan(k_jd_j)]\}Z_j$, and $Z_{in}^0 = Z_1$. Then $\Delta OD = -2\ln|t^*/t_{ref}|$ and $\Delta\phi = \arctan\{\mathrm{Im}[t^*/t_{ref}]/\mathrm{Re}[t^*/t_{ref}]\}$, where the asterisk is used to denote the photoexcited medium.
(38) Meurer, B.; Heitmann, D.; Ploog, K. Phys. Rev. Lett. **1992**, *68*, 1371−1374.
(39) Smith, N. V. *Phys. Rev. B* **2001**, *64*, 155106.
(40) Brekhovskikh, L. M. *Waves in Layered Media*; Academic Press: New York, 1960.

NL0256210